Analyst

Accepted Manuscript

ROYAL SOCIETY OF CHEMISTRY

www.rsc.org/analyst

A chitosan-Au-hyperbranched polyester nanoparticles-based antifouling immunosensor for sensitive detection of carcinoembryonic antigen

Chong Sun[a,b], Lie Ma[a], Qiuhui Qian[a], Soniya Parmar[c], Wenbo Zhao*[,a], Bo Zhao[a], Jian Shen*[,a]

[a]*Jiangsu Collaborative Innovation Center of Biomedical Functional Materials, Jiangsu Key Laboratory of Biofunctional Materials,College of Chemistry and Materials Science, Nanjing Normal University, Nanjing 210023, PR China*

[b]*Key Laboratory for Soft Chemistry and Functional Materials of Ministry of Education, School of Chemical Engineering, Nanjing University of Science and Technology, Nanjing 210094, PR China*

[c]*Department of Biological Sciences and Bioengineering, Indian Institute of Technology, Kanpur 208016, India*

*Corresponding authors.

E-mail address: zhaowenbo@njnu.edu.cn, jshen@njnu.edu.cn

Tel: +86 25 85891536, Fax: +86 25 83598280

Abstract

Analysts are always interested in finding new functional nanomaterials and devices with good properties for electrochemical sensor applications. In this paper, hyperbranched polyester nanoparticles with carboxylic acid functional groups (HBPE-CA NPs) were synthesized and combined with chitosan wrapped around Au nanoparticles (CS-Au NPs) to prepare a novel and sensitive electrochemical immunosensor by adsorption of carcinoembryonic antibody (anti-CEA) on the (HBPE-CA)/CS-Au NPs modified glass carbon electrode (GCE). Under the optimized conditions, the proposed immunosensor

displayed a good amperometric response to carcinoembryonic antigen (CEA). Moreover, based on the antibiofouling properties, the immunosensor could be used for detection of CEA in whole blood directly, and exhibited a wide detection range (1 $fg \cdot mL^{-1}$-10^7 $fg \cdot mL^{-1}$), a low detection limit of 0.251 $fg \cdot mL^{-1}$ (signal/noise=3). Control experiments were also carried out by using ascorbic acid (AA), uric acid (UA), human immunoglobulin G (IgG), BSA and glucose in the absence of CEA. The good stability and repeatability of this immunosensor were also proved. Importantly, the results of the detection of clinical whole blood specimens with the proposed immunosensor were well consistent with the data determined by enzyme-linked immunosorbent assay (ELISA) in serum samples. Furthermore, the developed immunosensor could provides a promising immunoassay strategy for clinical applications for the values we measured in whole blood directly are more close to the real values probably.

Keywords: Electrochemical Immunosensor, Hyperbranched Polyester Nanoparticles, Chitosan-Au Nanoparticles, Whole Blood, Antibiofouling, Carcinoembryonic Antigen Detection

1. Introduction

Different tumor markers, which indicate particular disease processes, are used in oncology to help detect the presence of cancer.[1-7] Among them, carcinoembryonic antigen (CEA) is one of the most widely used tumor markers worldwide associated with liver, colon, breast and colorectal cancer. So the sensitive detection of CEA plays an important role in early monitoring and screening disease recurrence, and can improve the longterm survival of cancer patients.[8-11]

In recent years, many methods that address the issue have been proposed.[7,12-16] Zhang et al. reported a protocol involving the electropolymerization of o-aminobenzoic acid (o-ABA) on a glass carbon electrode (GCE) to form a poly(o-ABA) (PAB) film which was covalently linked to capture carcinoembryonic antibody (anti-CEA) *via* N-ethyl-N'-(3-dimethylaminopropyl) carbodiimide (EDC) and N-hydroxysuccinimidobiotin (NHS). The detection limit of CEA was 2×10^{-3} ng·mL^{-1}.[17] Lin et al. summarized many chemiluminescence assays to determine different tumor markers.[14] Our group also described a new electrochemical immunosensor electrode using ATRP method to prepare P(PEGMA) polymer brushes for immobilization of anti-CEA. The P(PEGMA) polymer brushes provided more stable chemical bonds with anti-CEA, which ensured the tumor marker to be covalently linked to the ITO electrode. This proposed immunosensor showed a good linear range and satisfactory selectivity.[18]

But until now, these above traditional eletrochemical or chemiluminescence methods that applied for detection of CEA concentration have obvious defects. The final data of CEA level were obtained from serum samples, not original whole blood of the inspected person. It means the test results are not precise. Besides, the serum is

obtained by collecting whole blood and centrifugating. These additional instruments, such as centrifuging machine, become necessary, but it is not convenient for small community clinic or on-line detection.

However, it is very difficult to design and prepare a electrochemical immunosensor that can be used in whole blood directly because the biofouling of electrode surface can be developed by platelet, fibrin and blood cell adhesion in whole blood media.[19,20]

Analysts are always interested in finding new functional materials with good properties to improve the behavior of electrochemical immunosensor. Hyperbranched polymers have attracted significant attention for their unique architecture and novel properties including good solubility, special viscosity behavior, and high density of their functional groups.[21,22] Owing to the unique architecture of hyperbranched polymers, the multifunctional groups properties can be utilized to construct biosensor electrode by the chemical modification of the terminal-groups.[23,24]

In this paper, we have synthesized hyperbranched polyester nanoparticles with carboxylic acid functional groups (HBPE-CA NPs) for immobilization of anti-CEA, and developed a novel electrochemical immunosensor for detecting CEA. As far as we know, this is the first report that hyperbranched polyester nanoparticles were used to modify the electrode surface for preparing electrochemical immunosensor which can be applied in the detection of CEA. More details of preparation of electrode that modified by hyperbranched polyester nanoparticles, the electrochemical detection and analysis were presented.

2. Experimental

2.1. Reagents

CEA and anti-CEA were purchased from Nanjing Senbeijia Biotechnology Co., Ltd (China) and stored at 4 ℃ before use. Human immunoglobulin G (IgG), EDC and NHS were purchased from Sigma-Aldrich Co. (USA), β-D-(+)-glucose (99%) was obtained from J&K Chemical Co. Inc. (China). Hydrogen tetrachloroaurate (Ⅲ) trihydrate ($HAuCl_4 \cdot 3H_2O$, 99.9%) was obtained from Alfa Aesar, a Johnson Matthey Company. Chitosan (CS) and bull serum albumin (BSA) were obtained from Aladdin Chemistry Co. Ltd. (China). Butanedioic anhydride was purchased from Energy Chemical Co. Ltd. (China). Triethylamine and tetrahydrofuran (THF) were purchased from Sinopharm Chemical reagent Co. Ltd. (China) and refluxed with CaH_2 and sodium respectively, then distilled prior to use. Phosphate buffer solutions (PBS) with various pHs were prepared with 0.1 M KH_2PO_4 and 0.1 M Na_2HPO_4 solutions containing 0.1 M KCl as the supporting electrolyte. All other chemicals were of analytical grade and were used as received. All solutions were prepared with double-distilled water (ddH_2O).

2.2. Synthesis of HBPE-CA NPs

The HBPE-CA NPs were prepared as follows: 1.02 g hyperbranched polymer HBPE (0.87 mM -OH groups) was dissolved in 60 mL THF, then 2.07 g butanedioic anhydride and 1.0 mL triethylamine were dissolved in 40 mL THF and added into the polymer solution. The reaction mixtures were stirred at room temperature for 20 h.[25] Upon completion, white viscous products were filtrated on the bottom of the flask and the solvent was removed. After the viscous products were dissolved in ethanol and precipitated with THF for three times, the filtrate was washed by THF for several times, then the hyperbranched polyester HBPE-CA NPs were obtained. Yield 80%.

2.3. Apparatus

Atomic force microscopy (AFM) images were obtained by scanning probe microscopy (SPM, Vecco, USA). The morphology and structure of HBPE-CA NPs were characterized by transmission electron microscopy (TEM, HITACHI H-7650, Japan). The Zeta Potential (ζ) of HBPE-CA NPs was detected using a Nano ZS90 Zetasizer (Malvern, UK). The measurement is made in automatic mode, and the data were analysed using the software supplied by the manufacturer. The Fourier transform infrared (FTIR) spectra were collected in the reflectance mode using a NEXUS 670 FTIR spectrophotometer (Nicollet, USA) with an optical fiber in the range from 650 to 3800 cm^{-1}.

2.4. Preparation of the modified electrodes

GCE was successively polished on a mirror finish using 0.3 and 0.05 μm alumina slurry and then rinsed thoroughly with ddH_2O. After successive sonications in absolute alcohol and ddH_2O, the electrode was rinsed with ddH_2O and allowed to dry at room temperature. The preparation procedure was showed in Scheme 1. Firstly, the electrode was electro-deposited with CS wrapped around Au nanoparticles (CS-Au NPs) by applying a constant potential of -1.5 V for 180 s in a solution containing 0.5 $g{\cdot}L^{-1}$ CS (1% acetic acid as solvent) and 250 $mg{\cdot}L^{-1}$ $HAuCl_4$ solution, then the modified GCE were rinsed with ddH_2O to get CS-Au modified electrode. After that, 8 μL of 1 $mg{\cdot}mL^{-1}$ HBPE-CA was dropped onto the surface of CS-Au/GCE and kept overnight at 4 ºC. Thus, the HBPE-CA NPs were immobilized by electrostatic absorption, and (HBPE-CA)/CS-Au/GCE was obtained. Next, 5 mL of 400 mM EDC and 100 mM NHS in 0.1 M PBS (pH = 7.4) was applied to the (HBPE-CA)/CS-Au/GCE surface to activate the carboxyl groups.[26,27] After 2 h of incubation, the electrode was washed with ddH_2O

and then 10 μL anti-CEA (50 μg·mL^{-1}, PBS, pH = 7.4) was spread on the surface and kept overnight. In order to block possible remaining active sites of the electrode and to reduce the difference of electrical signals among every fabrications of immunosensor, the immunosensor were incubated with 5% BSA for 30 min at 37 °C, and washed with ddH_2O for three times. Finally, anti-CEA modified electrodes were incubated in 15 μL CEA standard solution with various concentrations in PBS buffer for 20 min at room temperature, followed by washing with pH = 7.4, 0.1 M PBS. Thus, the modified electrode of the resulting CEA/anti-CEA/(HBPE-CA)/CS-Au/GCE was recorded to produce the detection signal corresponding to the analyte.

2.5. Antibiofouling evalution of modified GCE surface

The antibiofouling property of the bare GCE and modified GCE surface was evaluated by whole blood adhesion test under *in vitro* conditions.

Whole blood adhesion tests are used to evaluate the blood compatibility of material surfaces.[28-30] Here, the surface sections of blank GCE, CS-Au/GCE, (HBPE-CA)/CS-Au/GCE and anti-CEA/(HBPE-CA)/CS-Au/GCE were placed in individual wells of a 24-well tissue culture plate and each well was equilibrated with 1.0 mL of PBS (pH = 7.4) for 24 h at 25 ºC. Then, each well was added with 1.0 mL of whole blood. After being incubated for 60 min at 37 ºC in humidified air, the samples were taken out. All the GCEs were rinsed for three times with PBS, then they were immersed into 2.5% glutaraldehyde for 30 min to fix the adhered blood cells, and rinsed three times with PBS. The GCEs were gradient-dried with ethanol-water solutions (50, 60, 70, 80, 90, 95, 100% (v/v)) for 30 min and dried in air.[28,30-33] Finally, the samples were sputter-coated with gold prior to observation under JEOL JSM-6300 scanning electron

microscope (SEM).

The coagulation assays were performed and measured by using a Semi automated Coagulometer (RT-2204C, Rayto, USA).

2.6. Electrochemical measurements

All electrochemical experiments were measured on a CHI 760D electrochemical workstation (Shanghai, China), a three-electrode electrochemical cell was composed of a modified glass carbon electrode (GCE, Φ = 3 mm) as the working electrode, a platinum wire as the auxiliary electrode, and a saturated calomel electrode (SCE) as the reference electrode. Cyclic voltammetry (CV) was performed in the potential between -0.4 and 0.8 V. The parameters applied in differential pulse voltammetry (DPV) were as follows: pulse amplitude of 50 mV, pulse width of 50 ms and voltage range from -0.3 to 0.6 V. The electrochemical impedance spectroscopy (EIS) tests were carried out in the frequency range of 1 Hz-100 kHz with a 5 mV AC amplitude. The data points were taken after 2 s quiet time (12 data points per frequency decade). All measurements were carried out at room temperature.

3. Results and discussion

3.1. Characterization of HBPE-CA NPs

TEM was performed to estimate the size and morphology of the HBPE-CA NPs. Typical TEM photographs showed that HBPE-CA NPs were well dispersed with an average diameter of 270 nm (Fig. S1). The ζ-potential of HBPE-CA NPs was -29.7 mV, and this negative potential also contribute to the carboxylic acid functional groups. Thus, the HBPE-CA NPs can be immobilized on the surface of CS-Au by electrostatic

absorption, and (HBPE-CA)/CS-Au/GCE was obtained.

Surface characterization by FTIR was carried out to verify whether HBPE-CA NPs were successfully grafted on CS-Au/GCE (Fig. 1). CS showed a distinct amide I band and amide II band at 1614 and 1520 cm^{-1}, respectively (curve a).[34-36] The spectra of HBPE-CA NPs grafted on CS-Au/GCE showed peaks at 1729 cm^{-1}, which are associated with symmetric υCOO^- vibrations, respectively (curve b).[37,38] And the high levels peaks at 1556 cm^{-1} include antisymmetric $\upsilon C=O$ in HBPE-CA NPs and amide II band in CS. These peaks confirmed that the HBPE-CA NPs were successfully grafted on CS-Au/GCE.

3.2. Antibiofouling evalution of the modified GCE surface

A thrombus is formed from the combination of mutually fused platelets plus the insoluble fibrin and the cells that it has trapped from the blood.[39] Platelet activation and fibrin formation are delicate processes that are under the control of many small physiological events.[40] Anti-fouling surfaces that exhibit low platelet adhesion are highly desirable in many biomedical applications as an anticoagulation idea.[41] Fig. 2 showed SEM pictures of blank GCE surface, the surface coated with CS-Au, (HBPE-CA)/CS-Au and anti-CEA/(HBPE-CA)/CS-Au after contact with whole blood for 60 min. Platelet deposition and blood cells were observed on the surface of blank GCE (Fig. 2A). In the case of the GCE's surface electro-deposited with CS-Au, numerous adherent blood cells and fibrin adhered on the surface as some aggregates because blood clots can be formed by CS (Fig. 2B). However, no blood cell adhesion was proved on the (HBPE-CA)/CS-Au modified GCE surfaces (Fig. 2C). Basing on the above observations and the coagulation assays (Fig. S2), it was believed that thrombus was difficult to form onto the

(HBPE-CA)/CS-Au modified GCE surfaces without fused platelets and cells. Moreover, platelet deposition and blood cell adhesion were suppressed on the GCE surface modified with anti-CEA/(HBPE-CA)/CS-Au (Fig. 2D). The results strongly indicated that thrombus were difficult to form onto the modified GCE surface. The good antithrombogenicity can be attributed to excellent water solubility and the pendant functional carboxylic acid groups with negative charge of the HBPE-CA NPs. Thus, platelet deposition and blood cell adhesion were suppressed and the modified GCE surface can create a good microenvironment when the detection was made in whole blood.

3.3. Optimization of the experimental parameters of the immunosensor

The sensitivity of the immunosensor is often related to some factors, such as the deposition time of CS-Au, pH value of PBS and interaction time of anti-CEA and CEA. These factors were optimized when the immunosensor was incubated in 10 $ng \cdot mL^{-1}$ CEA.

The influence of the deposition time on the peak current intensities was shown in Fig. 3A. The accumulation time onto GCE surface was varied from 80 to 200 s. As expected, the peak current increases with increasing accumulation time, however a plateau was reached after 180 s. When the deposition time was 180 s, the deposited CS-Au nanoparticles with uniform size could be well modified on the surface of GCE (Fig. S3). Thus, 180 s as accumulation time was chosen as a good compromise in subsequent analysis.

Since the pH of the working buffer would influence the electrochemical response of the immunosensor and the formation of immuno-complex on electrode surface, a series

of PBS with the pH values ranged from 5.0 to 8.0 were evaluated. As shown in Fig. 3B, the current responses increased with increasing pH values from 5.0 to 7.0 and then decreased when the pH was over 7.0. Compared to the data of response current obtained within other pH values regions, more larger response current was obtained within the range of pH 7.0 to 7.4. However, the normal pH values for arterial whole blood are 7.35 to 7.454; for venous whole blood, 7.36 to 7.41.[42] Thus, the buffer solution was adjusted to pH 7.4 and used in all experiments below.

The incubation time of the anti-CEA and CEA was also an important factor that affects the analytical performance of the proposed immunoassay. Fig. 3C revealed the influence of incubation time of the immunoassay. The current responses increased with the increasing incubation time and then started to level off at 20 min. Therefore, an incubation time of 20 min was selected for later assays.

3.4. Effect of scan rate

CV is used to study the (HBPE-CA)/CS-Au composite films behavior in 0.1 M PBS (pH=7.4). Both redox peak currents enlarged gradually with the increasing scan rate (Fig. S4). The reduction and oxidation peak currents were linearly proportional to the scan rate in the range from 20 to 300 $mV \cdot s^{-1}$ with the results as I_{pc} (μA) = 1.8067 + 0.0519 υ ($mV \cdot s^{-1}$) (r = 0.9956) and I_{pa} (μA) = -3.1307 – 0.0426 υ ($mV \cdot s^{-1}$) (r = 0.9927). It is evident that the increase in peak currents with the scan rate, keeping potential constant, suggests the occurrence of surface confined and reversible diffusion less redox transitions within the (HBPE-CA)/CS-Au film.[43]

3.5. Electrochemical characteristics of the immunosensor

In order to investigate the electrochemical properties of

anti-CEA/(HBPE-CA)/CS-Au/GCE, different modified electrodes were recorded by cyclic voltammogram. Fig. 4A showed the CVs of different electrodes at a scan rate of 100 $mV \cdot s^{-1}$, after immobilization of anti-CEA and after incubation of the later in CEA solution for 20 min. As shown in curve a, anti-CEA modified CS-Au deposited GCE exhibited a pair of redox peaks. Compared with anti-CEA/CS-Au/GCE (curve a), anti-CEA/(HBPE-CA)/CS-Au/GCE (curve b) displayed a pair of well-defined and quasi-reversible CV peak with a formal potential value ($E^{0'}$) of 0.196 V. The current signal of the redox peaks at anti-CEA/(HBPE-CA)/CS-Au/GCE were more larger, stable and quasi-reversible. Upon incubation with CEA solution, the peak current decreased greatly (curve c), suggesting an obvious steric hindrance process for the binding of CEA to the surface of the anti-CEA/(HBPE-CA)/CS-Au/GCE.

EIS was carried out to characterize the impedance change of the electrode surface in the modification process. In EIS, the semi-circle diameter equals the interface electron-transfer resistance (R_{et}), which controls the electron-transfer kinetics of the redox probe at the electrode interface. Fig. S5 illustrated the typical nyquist diagram at the bare GCE (a), CS-Au/GCE (b), (HBPE-CA)/CS-Au/GCE (c) and anti-CEA/(HBPE-CA)/CS-Au/GCE (d) in 10 mM $[Fe(CN)_6]^{3-/4-}$(1:1) solution containing 0.1 M KCl. Curve a in Fig. S5 showed the electrochemical impedance spectrum of the bare GCE, implying a very low electron transfer resistance to the redox-probe dissolved in the electrolyte solution. The CS-Au/GCE decreased the R_{et} tremendously (curve b), because Au can improve the conductivity of the GCE and facilitates the electron transfer between solution and electrode interface. A bigger well defined semi-circle at high frequency regions was observed at (HBPE-CA)/CS-Au/GCE (curve c) compared with the

bare GCE (a), indicating that the non-conductivity of HBPE-CA NPs inhibited the electron transfer of the redox probe of $[Fe(CN)_6]^{3-/4-}$ to the electrode surface to some degree. Moreover, when anti-CEA was modified on the modified GCE (d), the R_{et} was much larger than other electrodes. The results demonstrated that anti-CEA has been successfully immobilized on the electrode surface.

3.6. Ameperometric determination in whole blood

DPV technique has a potential advantage to increase the sensitivity and selectivity in the process of detection.[44] Blood samples were supplied by volunteers. Fig. 4B showed the calibration curve obtained by measuring the DPV peak current intensity vs. logarithmic value of CEA concentration in whole blood. The measurements were repeated 3 times to obtain the standard deviation. A linear relationship between the current intensity and logarithmic value of CEA concentration could be found in the range of 1 $fg \cdot mL^{-1}$-10^7 $fg \cdot mL^{-1}$ in whole blood. The linear regression equation was I (μA) = -2.745 logc – 0.464 with a correlation coefficient of 0.9927. Inset in Fig. 4B showed DPV curves recorded on the anti-CEA/(HBPE-CA)/CS-Au/GCE in the presence of various CEA concentrations in whole blood. The detection limit for CEA concentration was estimated to be 0.251 $fg \cdot mL^{-1}$ (S/N = 3). To further highlight the merits of the electrochemical immunoassay, the analytical properties of the immunosensor were compared with those of other CEA electrochemical immunosensors.[45-51] Characteristics including the linear range and detection limit were summarized in Table S1 in the supplementary information.

3.7. Selectivity, stability and reproducibility

The selectivity and stability of the immunosensor were investigated with DPV

method. To further address the non-specific absorption of other biological molecules on the immunosensor, control experiments have been performed by adding possible interferents, such as ascorbic acid (AA), uric acid (UA), human immunoglobulin G (IgG), BSA and glucose, instead of CEA.[52] The modified GCE was immersed in the solution of 1 ng·mL^{-1} of each interferent for 30 min without the presence of CEA, respectively. Relative response in Fig. S6 was obtained by signals of the proteins dividing the signal of the CEA then multiplying 100%. It was found that these substances did not cause obvious interference in the determination of CEA in the presence of these interferents. Thus, the immunosensor based on anti-CEA/(HBPE-CA)/CS-Au/GCE has good anti-interferent ability.

The reproducibility of the immunosensor was evaluated from the DPV response of the anti-CEA/(HBPE-CA)/CS-Au/GCE. A series of six measurements from the batch resulted in a relative standard deviation (RSD) of 4.3%, indicating good electrode-to-electrode reproducibility of the fabrication protocol described above. On the other hand, the intra-assay precision of the immunosensor was estimated by assaying two CEA concentrations for six replicate measurements. At the CEA concentrations of 0.05 ng/mL and 5 ng/mL, the RSDs of intra-assay with this method were 5.9% and 6.5%, showing an acceptable precision. Since stability is a very important characteristic, it was necessary to check it for the developed immunosensor here. When the anti-CEA/(HBPE-CA)/CS-Au/GCE was stored in the refrigerator at 4 ℃, the DPV response retained 93.1% value of the initial response, showing a quite satisfying stability. Good stability can be attributed to the strong interactions between anti-CEA and CEA.

3.8. Real sample analysis

To investigate the reliability of the present immunosensor for real samples, three human blood samples were assayed using the present immunoassay and ELISA as a reference method (Table 1). The relative deviation between these two methods was from −5.2% to 3.8%. It was shown that the values measured in whole blood by the immunosensor were well consistent with the data determined by ELISA in serum samples. Furthermore, the values we measured in whole blood directly are more close to the real values probably. Thus, the developed immunosensor could be practically applied in clinical analysis to detect the concentration of CEA.

4. Conclusion

In this paper, a novel and sensitive CEA amperometric immunosensor was successfully fabricated simply by immobilizing anti-CEA on the HBPE-CA and CS-Au NPs. HBPE-CA NPs we proposed here have many advantages such as their unique architecture, novel properties including good solubility and high density of their functional groups. The electrochemical immunosensor could be applied in whole blood directly that attributed to antibiofouling electrode surface. The immunosensor exhibited a low detection limit of 0.251 $fg \cdot mL^{-1}$, and a linear calibration plot was obtained in the wide concentration range from 1 $fg \cdot mL^{-1}$-10^7 $fg \cdot mL^{-1}$. This work might be of significance in clinic determination and will be investigated by more in-depth research in near future.

Acknowledgement

The work was supported by National-Local Joint Engineering Research Center for Biomedical Functional Materials, Natural Science Foundation of Jiangsu Province of China (BK 20131396), the Priority Academic Program Development of Jiangsu Higher

Education Institution, and Base of production, education & research of prospective joint research project of Jiangsu Province (BY2011109).

Appendix A. Supplementary material

References:

1 S. Benchimol, A. Fuks, S. Jothy, N. Beauchemin, K. Shirota and C.P. Stanners, *Cell,* 1989, **57**, 327-334.

2 C. Ilantzis, L. Demarte, R.A. Screaton and C.P. Stanners, *Neoplasia,* 2002, **4**, 151-163.

3 J. Schneider, H.G. Velcovsky, H. Morr, N. Katz, K. Neu and E. Eigenbrodt, *Anticancer Res.,* 2000, **20**, 5053-5058.

4 F. Tan, A. Aydiner, E. Topuz, V. Yasasever, A. Karadeniz and P. Saip, *J. Exp. Clin. Can. Res.,* 2000, **19**, 477-481.

5 D.T. Kiang, L.J. Greenberg and B.J. Kennedy, *Can. J,* 1990, **65**, 193-199.

6 F. Safi, I. Kohler, E. Rottinger and H.G. Beger, *Cancer,* 1991, **68**, 574-582.

7 I.I. Suni, *Trends Analy. Chem.,* 2008, **27**, 604-611.

8 G. Sun, J. Lu, S. Ge, X. Song, J. Yu, M. Yan and J. Huang, *Anal. Chim. Acta,* 2013, **775**, 85-92.

9 V. Kulasingam and E.P. Diamandis, *Nat. Clin. Pract. Oncol.,* 2008, **5**, 588-599.

10 X. Sun and Z. Ma, *Anal. Chim. Acta,* 2013, **780**, 95-100.

11 Y. Cai, H. Li, Y. Li, Y. Zhao, H. Ma, B. Zhu, C. Xu, Q. Wei, D. Wu and B. Du, *Biosens. Bioelectron.,* 2012, **36**, 6-11.

12 R. Yuan, Y. Zhuo, Y.Q. Chai, Y. Zhang and A.L. Sun, *Sci. China Ser. B,* 2007, **50**, 97-104.

13 J. Wang, *Biosens. Bioelectron.,* 2006, **21**, 1887-1892.

14 J. Lin and H. Ju, *Biosens. Bioelectron.*, 2005, **20**, 1461-1470.

15 I.E. Tothill, *Semin. Cell Dev. Biol.,* 2009, **20**, 55-62.

16 C.B. Jacobs, M.J. Peairs and B.J. Venton, *Anal. Chim. Acta,* 2010, **662**, 105-127.

17 Y.Y. Zhang, Y. Xiang, Y.Q. Chai, R. Yuan, X.Q. Qian and H.X. Zhang, *Sci. China Chem.,* 2011, **54**, 1770-1776.

18 X. Wang, M. Zhou, Y. Zhu, J. Miao, C. Mao and J. Shen, *J. Mater. Chem. B,* 2013, **1**, 2132-2138.

19 N. Wisniewski and M. Reichert, *Colloid. Surf. B,* 2000, **18**, 197-219.

20 C. Sun, X. Chen, Q. Han, M. Zhou, C. Mao, Q. Zhu and J. Shen, *Anal. Chim. Acta.,* 2013, **776**, 17-23.

21 M. Ahmed and R. Narain, *Biomaterials,* 2012, **33**, 3990-4001.

22 Y.B. Kim, H.K. Kim, H. Nishida and T. Endo, *Macromol. Mater. Eng.,* 2004, **289**, 923- 926.

23 Y. Xiao, H. Hong, A. Javadi, J.W. Engle, W. Xu, Y. Yang, Y. Zhang, T.E. Barnhart, W. Cai and S. Gong, *Biomaterials,* 2012, **33**, 3071-3082.

24 D. Foix, A. Serra, L. Amparore and M. Sangermano, *Polymer,* 2012, **53**, 3084-3088.

25 N.E. Ikladious, J.N. Asaad and N.N. Rozik, *Des. Monomers Polym.,* 2009, **12**, 469-481.

26 P. Wang, K. Tan, E. Kang and K. Neoh, *J. Mater. Chem,* 2001, **11**, 2951-2957.

27 G. Yasayan, A. Saeed, F. Francisco, S. Allen, M. Davies and A. Jangher, *Polym. Chem.,* 2011, **2**, 1567-1578.

28 C. Mao, L.C. Jiang, W.P. Luo, H.K. Liu, J.C. Bao, X.H. Huang and J. Shen, *Macromolecules,* 2009, **42**, 9366-9368.

29 C. Mao, C.X. Liang, W.P. Luo, J.C. Bao, J. Shen, X. Hou and W.B. Zhao, *J. Mater. Chem.,* 2009, **19**, 9025-9029.

30 H. Hu, X.B. Wang, S.L. Xu, W.T. Yang, F.J. Xu, J. Shen and C. Mao, *J. Mater. Chem.,* 2012, **22**, 15369-15369.

31 C. Mao, C.X. Liang, Y.Q. Mao, L. Li, X.M. Hou and J. Shen, *Colloid. Surf. B,* 2009, **74**, 362-365.

32 S. Alibeik, H. Sheardown, A.S. Rizkalla and K. Mequanint, *J. Biomat. Sci-Polym. E.,* 2007, **18**, 1195-1210.

33 P. Molina, J. Alcántara and C. López-Leonardo, *Tetrahedron,* 1997, **53**, 3281-3286.

34 M. Mucha, J. Piekielna and A. Wieczorek, *Macromol. Symp.,* 1999, **144**, 391-412.

35 G. Socrates, Infrared Characteristic Group Frequencies, Tables and charts, John Wiley and sons: Chichester, U.K., 2nd ed., 1994.

36 P. Kolhe and R.M. Kannan, *Biomacromolecules,* 2003, **4**, 173-180.

37 J.M. Pérez-Donoso, J.P. Monrás, A.F. Quest, R.F. Aroca, T.G. Chasteen and C.C. Vásquez, *Plosone*, 2012, **7**, e30741.

38 V. Pilla, S.R. de Lima, A.A. Andrade, A.C.A. Silva and N.O. Dantas, *Chem. Phys. Lett.,* 2013, **580**, 130-134.

39 C. Mao, Y.Z. Qiu, H.B. Sang, H. Mei, A.P. Zhu, J. Shen and S.C. Lin, *Adv. Colloid Interface Sci.,* 2004, **110**, 5-17.

40 E. Pretorius and P. Humphries, *Ultrastruct Pathol.*, 2007, **31**, 77-83.

41 M. Liu, X.L. Yue, Z.F. Dai, L. Xing, F. Ma and N.Q. Ren, *Langmuir*, 2007, **23**, 9378-9385.

42 A. Waugh, A. Grant, Anatomy and Physiology in Health and Illness, Churchill Livingstone Elsevier, Dutch, 2007.

43 S. Radhakrishnan, C. Sumathi, A. Umar, S.J. Kim, J. Wilson and V. Dharuman, *Biosens. Bioelectron.,* 2013, **47**, 133-140.

44 W.C. Liao and J. Ho, *Anal. Chem.,* 2009, **81**, 2470-2476.

45 J. Han, Y. Zhou, Y.Q. Chai, L. Mao, Y.L. Yuan and R. Yuan, *Talanta,* 2011, **85**, 130-135.

46 G. Lai, F. Yan and H. Ju, *Anal. Chem.,* 2009, **81**, 9730-9736.

47 Q. Li, D. Tang, J. Tang, B. Su, J. Huang and G. Chen, *Talanta,* 2011, **84**, 538-546.

48 M. Liang, R. Yuan, Y. Chai, L. Min and Z. Song, *Mikrochim. Acta,* 2011, **172**, 373-378.

49 W.T. Shi and Z.F. Ma, *Biosens. Bioelectron.,* 2011, **26**, 3068-3071.

50 D.P. Tang, R. Yuan and Y.Q. Chai, *Anal. Chem.,* 2008, **80**, 1582-1588.

51 R.M. Wang, X. Chen, J. Ma and Z.F. Ma, *Sens. Actuators B,* 2013, **176**, 1044-1050.

52 J. Han, J. Ma and Z. Ma, *Biosens. Bioelectron.,* 2013, **47**, 243-247.

Legends for the figures:

Scheme 1. The preparation procedure of CEA/anti-CEA/(HBPE-CA)/CS-Au modified GCE.

Fig. 1. The FTIR spectrogram of (a) CS-Au, and (b) (HBPE-CA)/CS-Au.

Fig. 2. SEM images of (A) blank GCE substrate, (B) GCE substrate modified with CS-Au, (C) GCE substrate modified with (HBPE-CA)/CS-Au, and (D) GCE substrate modified with anti-CEA/(HBPE-CA)/CS-Au exposed to human whole blood for 60 min, respectively.

Fig. 3. Effects of (A) deposition time of CS-Au NPs, (B) pH of detection solution, and (C) incubation time on the peak current. One parameter changed while the others were under their optimal conditions and 10 $ng \cdot mL^{-1}$ CEA was used as an example.

Fig. 4. (A) CVs of (a) anti-CEA/CS-Au/GCE, (b) anti-CEA/(HBPE-CA)/CS-Au/GCE, and (c) CEA/anti-CEA/(HBPE-CA)/CS-Au/GCE in 0.1 M PBS (pH = 7.4). (B) The calibration plots of the anodic peak current response versus concentration of CEA with the immunosensor under optimal conditions. The insert shows the DPV plots upon the addition of varying amounts of CEA ((a) 0, (b) 1 $fg \cdot mL^{-1}$, (c) 10 $fg \cdot mL^{-1}$, (d) 10^2 $fg \cdot mL^{-1}$, (e) 10^3 $fg \cdot mL^{-1}$, (f) 10^4 $fg \cdot mL^{-1}$, (g) 10^5 $fg \cdot mL^{-1}$, (h) 10^6 $fg \cdot mL^{-1}$, (i) 10^7 $fg \cdot mL^{-1}$, and (j) 10^8 $fg \cdot mL^{-1}$).

Table 1. Comparison of two methods obtained in practical samples.

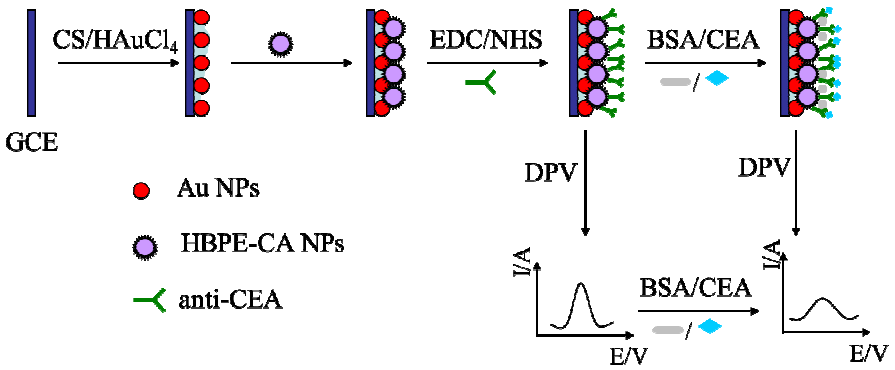

Scheme 1. The preparation procedure of CEA/anti-CEA/(HBPE-CA)/CS-Au modified GCE.

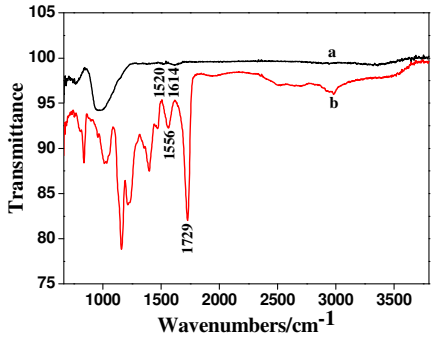

Fig. 1. The FTIR spectrogram of (a) CS-Au, and (b) (HBPE-CA)/CS-Au.

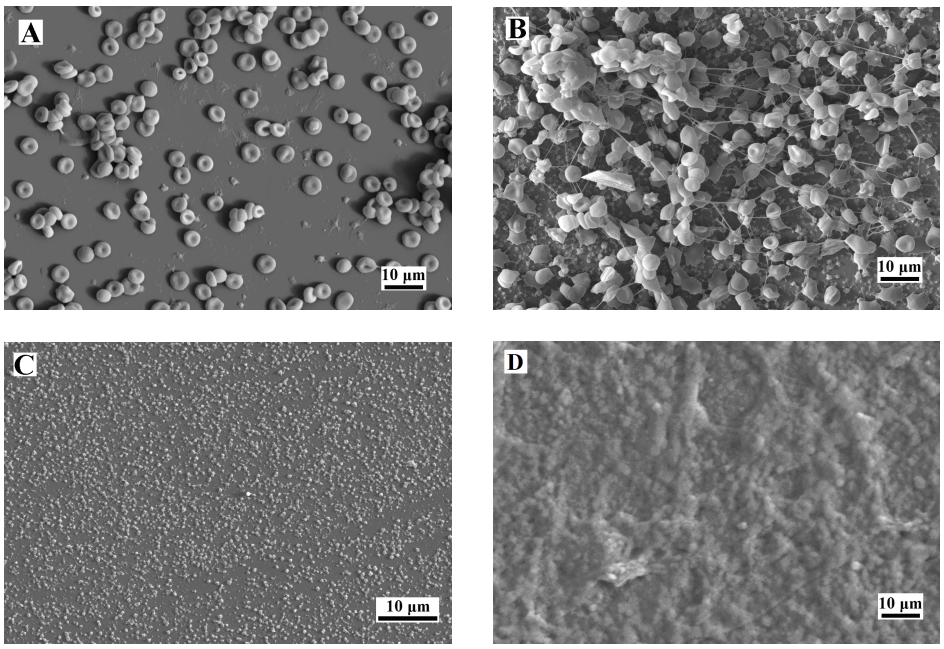

Fig. 2. SEM images of (A) blank GCE substrate, (B) GCE substrate modified with CS-Au, (C) GCE substrate modified with (HBPE-CA)/CS-Au, and (D) GCE substrate modified with anti-CEA/(HBPE-CA)/CS-Au exposed to human whole blood for 60 min, respectively.

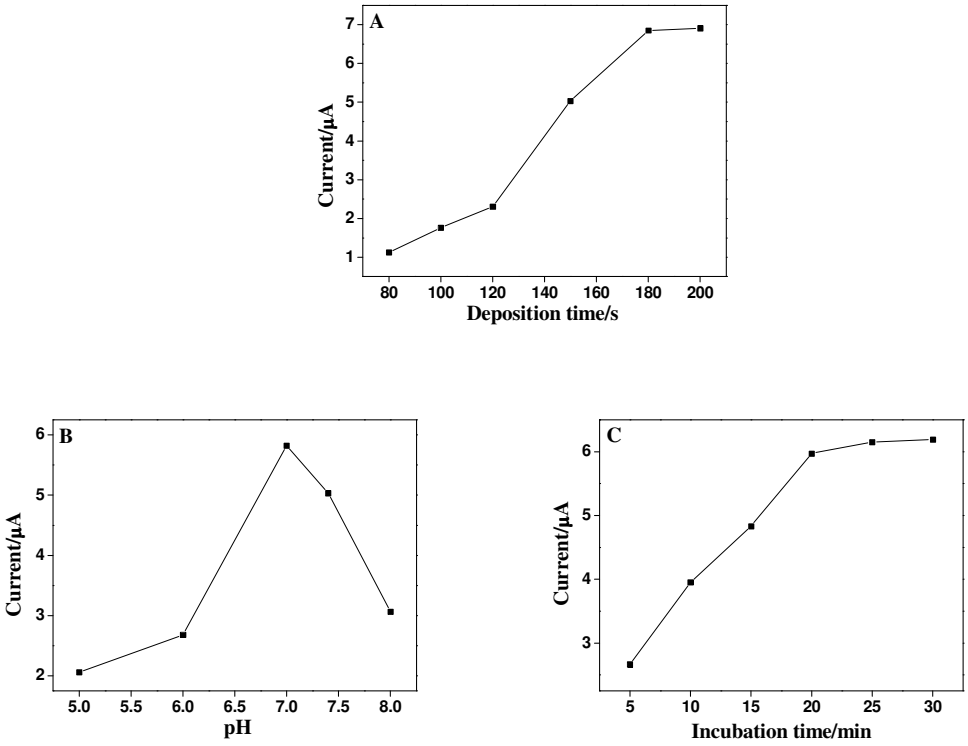

Fig. 3. Effects of (A) deposition time of CS-Au NPs, (B) pH of detection solution, and (C) incubation time on the peak current. One parameter changed while the others were under their optimal conditions and 10 ng·mL^{-1} CEA was used as an example.

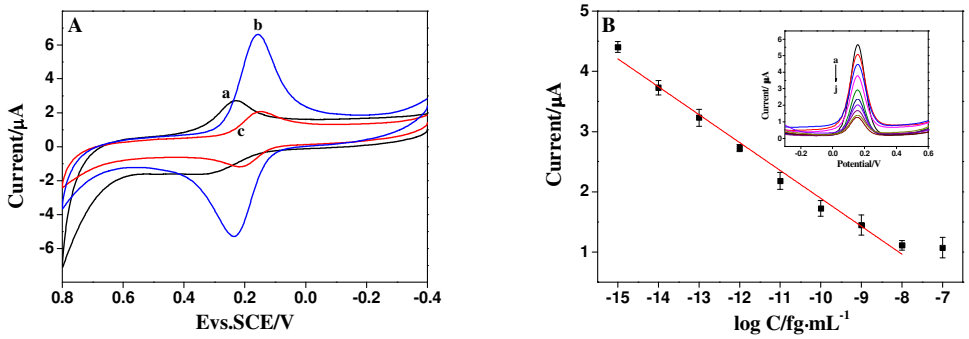

Fig. 4. (A) CVs of (a) anti-CEA/CS-Au/GCE, (b) anti-CEA/(HBPE-CA)/CS-Au/GCE, and (c) CEA/anti-CEA/(HBPE-CA)/CS-Au/GCE in 0.1 M PBS (pH = 7.4). (B) The calibration plots of the anodic peak current response versus concentration of CEA with the immunosensor under optimal conditions. The insert shows the DPV plots upon the addition of varying amounts of CEA ((a) 0, (b) 1 $fg \cdot mL^{-1}$, (c) 10 $fg \cdot mL^{-1}$, (d) 10^2 $fg \cdot mL^{-1}$, (e) 10^3 $fg \cdot mL^{-1}$, (f) 10^4 $fg \cdot mL^{-1}$, (g) 10^5 $fg \cdot mL^{-1}$, (h) 10^6 $fg \cdot mL^{-1}$, (i) 10^7 $fg \cdot mL^{-1}$, and (j) 10^8 $fg \cdot mL^{-1}$).

Table 1. Comparison of two methods obtained in practical samples.

Samples	1	2	3
ELISA ($ng \cdot mL^{-1}$)	1.35	5.81	8.14
Immunosensors ($ng \cdot mL^{-1}$)	1.28	5.75	7.90
Relative deviation (%)	3.8	2.3	-5.2

A chitosan-Au-hyperbranched polyester nanoparticles-based antifouling immunosensor for sensitive detection of carcinoembryonic antigen

Chong Sun[a,b], Lie Ma[a], Qiuhui Qian[a], Soniya Parmar[c], Wenbo Zhao*[,a], Bo Zhao[a], Jian Shen*[,a]

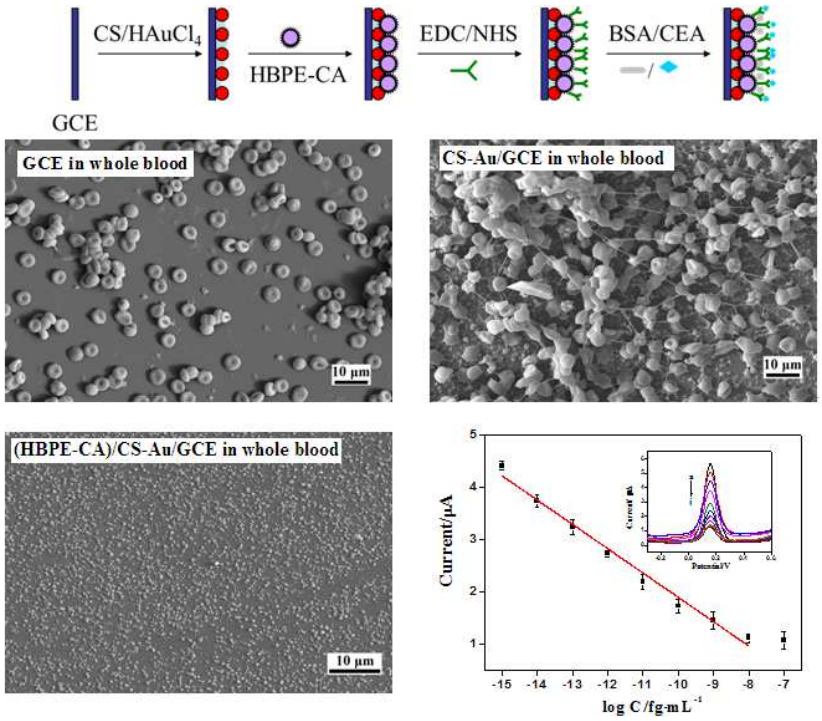

- A sensitive electrochemical immunosensor for the detection of carcinoembryonic antigen (CEA) was developed.
- The immunosensor was successfully used for CEA detection in whole blood based on the antibiofouling properties of carboxylic acid group functionalized hyperbranched polyester nanoparticles.
- The antibiofouling technique utilized for immunosensor might have potentially broad applications in whole blood diagnosis directly.